Journal of Fluids and Structures (1998) **12,** 655–676
Article No. fl980167

TWO-DIMENSIONAL TRANSONIC AEROELASTIC ANALYSIS USING THIN-LAYER NAVIER–STOKES METHOD§

B. B. Prananta
Faculty of Aerospace Engineering, Delft University of Technology Delft, The Netherlands

M. H. L. Hounjet
National Aerospace Laboratory, Amsterdam, The Netherlands

AND

R. J. Zwaan
Faculty of Aerospace Engineering, Delft University of Technology, Delft, The Netherlands

(Received 16 September 1997 and in revised form 7 May 1998)

A robust efficient upwind implicit time-marching algorithm for the two-dimensional unsteady Thin-Layer Navier–Stokes equations, employing subiterations, is presented, especially directed to the aeroelastic analysis in viscous transonic flow. The purpose of using subiterations is to accelerate steady-state convergence and to permit a large time step in time-accurate simulations, thereby reducing the computational cost, while maintaining adequate accuracy. The ability of the method is demonstrated for the cases of inherently unsteady flow due to shock-induced separation, forced vibrations with large time steps, $\mathcal{O}(10)$ per period, and an aeroelastic analysis of a two-degree-of-freedom airfoil.

1. INTRODUCTION

For more than a decade, time-marching aeroelastic solution procedures have been an important topic of research, primarily motivated by the steadily increasing attention to nonlinear aeroelastic phenomena, especially to the prediction of the decrease of aerodynamic damping occurring in transonic flow.

The early attempts to obtain a two-dimensional nonlinear time-marching aeroelastic method for transonic flow employed a transonic small disturbance (TSD) flow model. Most of these methods may be found in the systematic comparison of Edwards *et al.* (1982), which also describes an efficient integration method for coupled aeroelastic equations. From the many developments using the unsteady full-potential flow model, only a few time-marching aeroelastic solutions have been reported. The work of Ide & Shankar (1987) and Hounjet & Eussen (1994) are two of them. The application of the Euler equations for aeroelastic analysis in transonic flow was initiated by Bendiksen & Kousen (1987) with a modified explicit algorithm of Jameson. This development towards a more complex aerodynamic model was made possible not only by the advancements in CFD, but also by the availability

§This article is a revised version of the paper presented at the 1995 International Forum on Aeroelasticity and Structural Dynamics, 26–28 June 1995, Manchester, U.K.

0889–9746/060655–22 $30.00

of adequate computing power at a reasonable price. Later, Kousen & Bendiksen (1988) reported the possible occurrence of limit-cycle oscillations, which is a purely nonlinear phenomenon. Wu *et al.* (1989) presented time-marching aeroelastic results of two-dimensional configurations employing the Thin-Layer Navier–Stokes (TLNS) flow model. Guruswamy (1990) reported results for two-dimensional and three-dimensional configurations where the latter featured vortical flow.

These advancements in the time-marching aeroelastic analysis were mainly aiming at a better understanding of the transonic aeroelastic problem by applying physically refined unsteady aerodynamic models. Their applications are usually complex and expensive in terms of required computer resources. Aspects concerning industrial application, e.g. efficiency, cost and ease of usage, etc., have been hardly addressed. At the National Aerospace Laboratory in Amsterdam proper attention has been given to these aspects, with the development of the aeroelastic simulation method AESIM, based on the Clebsch potential; see Hounjet & Eussen (1994). The recent paper of Alonso & Jameson (1994) gives similar attention for a time-marching aeroelastic method employing the Euler flow model. These authors employ an implicit method based on the pioneering work of Jameson (1991), which allows the use of relatively large time steps while maintaining temporal accuracy. It is shown that the method has gained efficiency in time-marching aeroelastic analysis through its ability to march with large time steps. Later Alonso *et al.* (1995) also presented time-marching aeroelastic results using the Navier–Stokes flow model.

In this paper, an alternative time-marching aeroelastic method employing the Euler/Navier–Stokes flow models is presented, which has a capability of marching with time steps solely determined by the physics and not by stability considerations. The Euler/TLNS equations are solved using an unfactored implicit method employing a relaxation technique for the subiterations. The aero-structural equations are solved using the Newmark method. Contrary to the method of Jameson (1991), the present method is not critical to acceleration techniques (e.g. multigrid, local time stepping and residual averaging).

The two-dimensional work presented in this paper serves also as a pilot work in the development of a three-dimensional computational aeroelastic simulation method which has recently been presented in Prananta & Hounjet (1996) and Prananta & Hounjet (1997). Similar work on three-dimensional aeroelastic analysis using Euler/Navier–Stokes equations was presented by Guruswamy (1991), Rausch *et al.* (1992) and Lee-Rausch & Batina (1993). In Rausch *et al.* (1992), unstructured meshes are used and a temporal integration method employing point Gauss–Seidel relaxation is adopted. In Lee-Rausch & Batina (1993) and Guruswamy (1991) structured meshes are used and a first-order one-step temporal integration method is applied. The first employs an implicit approximate factorization method while the latter employs the LU-ADI method. The requirement for extension to three-dimensional configurations has primarily motivated the application of a temporal integration method employing a relaxation approach, like in Rausch *et al.* (1992), due to its favourable stability properties for two- and three-dimensional configurations. In combination with structured meshes a line relaxation is adopted for a faster convergence. To allow large time stepping, second- and third-order temporal integration methods are applied in the present work.

In the following sections, the techniques which are incorporated in the computational method will be discussed. Prior to aeroelastic applications, the method will first be validated for steady and unsteady flow simulations. In order to investigate the effect of viscosity on the aeroelastic behaviour at transonic speeds, results of aeroelastic simulations are presented with the aerodynamic part in the Euler as well as in the Navier–Stokes mode.

2. AERODYNAMIC MODEL

For flows at high Reynolds number, the viscous effects are concentrated in a layer close to the solid boundary, for which the Thin-Layer assumption is appropriate. In streamwise direction, where the convective behavior is dominant, the viscous terms are neglected. The governing equations are transformed from the Cartesian physical domain to a uniform computational domain as $\xi = \xi(x, z, t)$, $\zeta = \zeta(x, z, t)$ and $\tau = t$. In a curvilinear coordinate system, the TLNS equations can be written in a conservative form as

$$\frac{\partial \hat{Q}}{\partial \tau} + \frac{\partial \hat{E}}{\partial \xi} + \frac{\partial \hat{G}}{\partial \zeta} = \frac{\partial \hat{G}_v}{\partial \zeta}, \tag{1}$$

where the conservative variable is $\hat{Q} = hQ$, $Q = [\rho, \rho u, \rho w, \rho E]^{\mathrm{T}}$, and the inviscid flux vectors are

$$\hat{E} = \begin{bmatrix} \rho\hat{U} \\ \rho u\hat{U} + \hat{\xi}_x p \\ \rho w\hat{U} + \hat{\xi}_z p \\ \rho E\hat{U} + \hat{U}' p \end{bmatrix}, \quad \hat{G} = \begin{bmatrix} \rho\hat{W} \\ \rho u\hat{W} + \hat{\zeta}_x p \\ \rho w\hat{W} + \hat{\zeta}_z p \\ \rho E\hat{W} + \hat{W}' p \end{bmatrix}. \tag{2}$$

$\hat{U}$ and $\hat{W}$ are the contravariant velocities, while $\hat{U}' = \hat{U} - \hat{\xi}_t$ and $\hat{W}' = \hat{W} - \hat{\zeta}_t$ are the contravariant velocities on a fixed mesh. The hat ($\hat{}$) denotes an unscaled quantity (some metrics and velocities) with respect to $h = J^{-1}$. It should be noted that the conservative form of the governing equations in the transformed coordinate system are obtained by assuming the following transformation invariants are satisfied:

$$\frac{\partial \hat{\xi}_x}{\partial \xi} + \frac{\partial \hat{\zeta}_x}{\partial \zeta} = 0, \qquad \frac{\partial \hat{\xi}_z}{\partial \xi} + \frac{\partial \hat{\zeta}_z}{\partial \zeta} = 0, \tag{3}$$

$$\frac{\partial h}{\partial \tau} + \frac{\partial \hat{\xi}_t}{\partial \xi} + \frac{\partial \hat{\zeta}_t}{\partial \zeta} = 0. \tag{4}$$

Equation (4) is usually called the geometric conservation law, e.g. in Thomas & Lombard (1979) and Obayashi (1992). To avoid nonphysical sources in the discretized equations, equations (3, 4) have to be satisfied by the discretization method. According to the thin-layer assumption the viscous term $\hat{G}_v$ can be written in a very simple form as compared to the one often presented in the literature, namely,

$$\hat{G}_v = \frac{\mu}{\mathrm{Re}} \begin{bmatrix} 0 \\ m_1 u_\zeta + m_2 w_\zeta \\ m_2 u_\zeta + m_3 w_\zeta \\ \dfrac{m_1}{2}(u^2)_\zeta + m_2(uw)_\zeta + \dfrac{m_3}{2}(w^2)_\zeta + m_4 \dfrac{\gamma}{\mathrm{Pr}} \mathrm{e}_\zeta \end{bmatrix}, \tag{5}$$

where the flow variables have been separated from the metrics to facilitate the calculation of the Jacobian. In equation (5) the Stokes hypothesis for bulk viscosity is used where $\lambda + 2\mu/3 = 0$ and all derivatives in ξ direction have been dropped. The metric functions m_1–m_4 are

$$m_1 = (\tfrac{4}{3}\hat{\zeta}_x\zeta_x + \hat{\zeta}_z\zeta_z), \quad m_2 = \tfrac{1}{3}\hat{\zeta}_x\zeta_z, \quad m_3 = (\hat{\zeta}_x\zeta_x + \tfrac{4}{3}\hat{\zeta}_z\zeta_z), \quad m_4 = (\hat{\zeta}_x\zeta_x + \hat{\zeta}_z\zeta_z).$$

The density has been nondimensionalized by ρ_∞, the velocity by a_∞, the pressure by $\rho_\infty a_\infty^2$, the energy per unit mass by a_∞^2, the coefficient of viscosity by μ_∞, and the coordinators by T_c. The perfect gas relation is used to close the equations by relating the pressure to other flow variables by $p = (\gamma - 1)\rho[E - 1/2(u^2 + w^2)]$. For turbulent flow calculations, Reynolds averaging is applied and density-weighted mean turbulent variables are used. Following the eddy viscosity concept, the dynamic viscosity μ and the heat conduction coefficient have laminar and turbulent contributions:

$$\mu = \mu_{\mathrm{L}} + \mu_{\mathrm{T}} \quad \text{and} \quad \frac{k}{C_p} = \frac{\mu_{\mathrm{L}}}{\mathrm{Pr}_{\mathrm{L}}} + \frac{\mu_{\mathrm{T}}}{\mathrm{Pr}_{\mathrm{T}}}. \tag{6}$$

The laminar contribution is obtained through the use of Sutherland's law for molecular viscosity, while the turbulent contribution is obtained from the algebraic turbulence model of Baldwin & Lomax (1978). The Prandtl number is taken to be constant, $\mathrm{Pr}_{\mathrm{L}} = 0{\cdot}72$ and $\mathrm{Pr}_{\mathrm{T}} = 0{\cdot}90$.

Equation (1) is discretized using a cell-centred finite-volume method:

$$\frac{\partial}{\partial \tau} \int_{\mathscr{V}} hQ \, \mathrm{d}\xi \, \mathrm{d}\zeta + \int_{\partial \mathscr{V}} (\hat{E}, \hat{G} - \hat{G}_v)^{\mathrm{T}} \cdot (\mathrm{d}\xi, \mathrm{d}\zeta)^{\mathrm{T}} = 0. \tag{7}$$

By defining flux $\hat{E}$ on cell face $(i \pm \frac{1}{2}, j)$ and flux $(\hat{G} - \hat{G}_v)$ on cell face $(i, j \pm \frac{1}{2})$, the semi-discretized equations in a uniform computational domain read

$$h^{n+1}\frac{\partial Q}{\partial \tau} + Q^n \frac{\partial h}{\partial \tau} + \hat{E}^{n+1}_{i+1/2,j} - \hat{E}^{n+1}_{i-1/2,j} + (\hat{G} - \hat{G}_v)^{n+1}_{i,j+1/2} - (\hat{G} - \hat{G}_v)^{n+1}_{i,j-1/2} = 0, \tag{8}$$

where Q represents a cell-averaged value of the conservative variable. $\partial h/\partial \tau$ is calculated from the contravariant grid speed using equation (4). For a strictly A-stable scheme, at most second-order-accurate discretization may be applied for $\partial Q/\partial \tau$. The second-order scheme gives satisfactory results in most cases and is the default scheme of the present method. However, third-order-accurate backward differencing for $\partial Q/\partial \tau$, which is defined as stiffly stable by Gear (1971), is also applied for some results presented here. Although the stability region of a stiffly stable scheme does not cover the imaginary axis, it should not cause problems since an upwind scheme is applied for the spatial discretization.

The contravariant grid speed is calculated from the deformation of the mesh caused by the motion of the airfoil. This motion is prescribed in case of forced vibration, and for an aeroelastic simulation case it is determined by the solution of the elasto-mechanical equations. Here the elasto-mechanical equations are solved using a two-level scheme, viz., the Newmark method. In this case, the contravariant grid speed at a cell face, $\hat{\xi}_t^{n,n+1}$ or $\hat{\zeta}_t^{n,n+1}$, is calculated on the "space–time" area formed by a cell face at two structural levels. For a three-level scheme, e.g. the second-order implicit backward Euler scheme, the contravariant grid speed is calculated as

$$\hat{\xi}_t = \tfrac{3}{2}\,\hat{\xi}_t^{n,n+1} - \tfrac{1}{2}\,\hat{\xi}_t^{n-1,n}, \qquad \hat{\zeta}_t = \tfrac{3}{2}\,\hat{\zeta}_t^{n,n+1} - \tfrac{1}{2}\,\hat{\zeta}_t^{n-1,n}.$$

This way of calculating the contravariant grid speed was shown by Obayashi (1992) to be consistent with the rate of change of the cell volume which implies equation (4) is implicitly satisfied.

2.1. Inviscid Flux

The choice of the inviscid flux discretization between central and upwind method is mainly determined by the requirement of the present time integration method. Since relaxation is

applied in each time step, a well-conditioned Jacobian matrix is required. Discretization using an upwind method will result in a diagonally dominant Jacobian matrix. The importance to apply a high-resolution scheme for the inviscid part of the Navier–Stokes equations was discussed by Swanson & Turkel (1993). Flux difference splitting (FDS) meets this requirement and is thus applied in this study, where the approximate Riemann solver of Roe (1981) is employed. Roe's method, which is based on a special linearization of the Euler equations, is computationally simple and easy to extend to moving grid problems. Roe's FDS is also known to be insensitive to grid stretching, commonly involved in Navier–Stokes calculations.

The flux at a cell face is calculated from the solution of a locally one-dimensional Riemann problem. For instance, the flux in ξ direction, thus at cell face $(i \pm \frac{1}{2}, \mathrm{j})$, is

$$\hat{E} = \tfrac{1}{2}\,[\hat{E}(Q^+) + \hat{E}(Q^-)] - \tfrac{1}{2}\,|\hat{A}(\bar{Q})|(Q^+ - Q^-), \tag{9}$$

where the geometrical data at the cell face are used. Q^+ and Q^- are the states on the two sides of the cell face. $\bar{Q} = \bar{Q}(Q^+, Q^-)$ is the state at the cell face calculated using Roe's averaging of Q^+ and Q^-, and $\hat{A} = \partial\hat{E}/\partial Q$ is the Jacobian of the flux. $|\hat{A}|$ is calculated as $R|\Lambda|L$, where the columns of R and the rows of L are the normalized right and left eigenvectors of $\hat{A}(\bar{Q})$, respectively. The matrix of the right eigenvectors is

$$R = \begin{bmatrix} 1 & 0 & 1 & 1 \\ u & \tilde{\xi}_z & u + \tilde{\xi}_x a & u - \tilde{\xi}_x a \\ w & -\tilde{\xi}_x & w + \tilde{\xi}_z a & w - \tilde{\xi}_z a \\ k & \bar{W} & H + \tilde{U}' a & H - \tilde{U}' a \end{bmatrix} \tag{10}$$

and the matrix of the left eigenvectors is

$$L = \begin{bmatrix} 1 - \bar{\gamma}k/a^2 & \bar{\gamma}u/a^2 & \bar{\gamma}w/a^2 & -\bar{\gamma}/a^2 \\ -\bar{W} & \tilde{\xi}_z & -\tilde{\xi}_x & 0 \\ \varrho(\bar{\gamma}k - a\tilde{U}') & \varrho(a\tilde{\xi}_x - \bar{\gamma}u) & \varrho(a\tilde{\xi}_z - \bar{\gamma}w) & \varrho\bar{\gamma} \\ \varrho(\bar{\gamma}k + a\tilde{U}') & -\varrho(a\tilde{\xi}_x + \bar{\gamma}u) & -\varrho(a\tilde{\xi}_z + \bar{\gamma}w) & \varrho\bar{\gamma} \end{bmatrix}, \tag{11}$$

where $k = \frac{1}{2}(u^2 + w^2)$, $\bar{\gamma} = (\gamma - 1)$, $\varrho = 1/(2a^2)$ and $\bar{W} = \tilde{\xi}_z u - \tilde{\xi}_x w$. The tilde ($\tilde{}$) represents a quantity normalized by $|\nabla\xi|$. Roe's averaging is applied to (ρ, u, w, H) and $a = \bar{\gamma}(H - k)$. The eigenvalues λ are $\hat{U}, \hat{U}, \hat{U} - a, \hat{U} + a$. It can be seen that the grid speed influences the flux difference through the eigenvalues. When the flux is evaluated using the value of Q adjacent to the cell face, the scheme is of first-order-accurate and "total variation diminishing" (TVD). To obtain a higher-order scheme while maintaining the TVD property, the states at the two sides of the face are obtained using the MUSCL variable extrapolation of Van Leer:

$$Q^{\pm}_{i \mp 1/2} = Q_i \mp \frac{s}{4}\,[(1 - \kappa s)\,\mathrm{d}Q_i^{\pm} + (1 + \kappa s)\,\mathrm{d}Q_i^{\mp}], \tag{12}$$

with $\mathrm{d}Q_i^+ = Q_{i+1} - Q_i$, $\mathrm{d}Q_i^- = Q_i - Q_{i-1}$ and $\kappa = -1$ for a second-order fully upwind scheme or $\kappa = \frac{1}{3}$ for a third-order upwind bias scheme. The function s serves as a limiter for higher-order gradients to preserve the monotone behaviour of the first-order scheme. There

are many proper choices for the limiters, here the one of van Albada is applied because of its continuous behaviour:

$$s = \frac{2\mathrm{d}Q^+\mathrm{d}Q^- + \varepsilon}{(\mathrm{d}Q^+)^2 + (\mathrm{d}Q^-)^2 + \varepsilon}\,. \tag{13}$$

The small number ε assures the limiter to have a correct behaviour in the smooth regions.

2.2. Boundary Conditions

All boundary conditions are imposed in an explicit manner. Owing to the fact that in each subiteration the boundary condition is updated, they should converge together with the flow equations. At the airfoil surface the normal velocity vanishes for the inviscid case, and for the viscous case the tangential velocity vanishes as well. The pressure on the airfoil surface in the inviscid case is obtained through the normal momentum equation,

$$(\hat{\zeta}_x\hat{\xi}_x + \hat{\zeta}_z\hat{\xi}_z)\frac{\partial p}{\partial \xi} + (\hat{\zeta}_x^2 + \hat{\zeta}_z^2)\frac{\partial p}{\partial \zeta} = \rho h|\nabla\hat{\zeta}|\left(\frac{\partial \tilde{\zeta}_t}{\partial \tau} + u\frac{\partial \tilde{\zeta}_x}{\partial \tau} + w\frac{\partial \tilde{\zeta}_z}{\partial \tau}\right) + \rho\hat{U}|\nabla\hat{\zeta}|\left(\frac{\partial \tilde{\zeta}_t}{\partial \xi} + u\frac{\partial \tilde{\zeta}_x}{\partial \xi} + w\frac{\partial \tilde{\zeta}_z}{\partial \xi}\right). \tag{14}$$

For viscous flow, a zero normal pressure gradient is prescribed, which is approximated simply as $\partial p/\partial\zeta = 0$.

At the outer boundary, far from the airfoil, the flow is practically inviscid, so that boundary conditions for the Euler equations are applied. The locally one-dimensional boundary condition based on Riemann invariants is applied.

2.3. Time-Stepping Method

The classical one-step method employing approximate factorization, which is efficient for steady flow calculations, reveals limitations in both stability and accuracy for unsteady flow applications. The stability is known to be limited by the factorization error which becomes even worse in the case of three-dimensional flow. The accuracy limitation stems from the fact that, in each time step, only a linearized equation is solved. This means that the nonlinear equation is satisfied only at the steady level. To allow large time steps while sustaining accuracy, both deficiencies have to be resolved. In the present study an unfactored method is employed for solving the discretized equations which removes the stability limit, and subiterations are employed at each time step to satisfy the nonlinear unsteady equations.

The residual at a time level is defined by equation (8). The subiteration scheme is obtained via Newton's method:

$$\frac{\partial R(Q^p)}{\partial Q}\,\Delta Q^p = -\,R(Q^p, Q^n, Q^{n-1}), \tag{15}$$

where p is the subiteration level, Q^p is the approximation to Q^{n+1} and ΔQ^p is $Q^{p+1} - Q^p$. The accuracy of the subiteration scheme is determined only by the right-hand side (Rhs), while the left-hand side (Lhs) determines the rate of convergence. Quadratic convergence of the Newton's method is obtained if the Lhs is the exact Jacobian of the Rhs and inverted

exactly to obtain the correction. An inexact Lhs and an approximate inversion may be used for obvious reasons, at the cost of losing the quadratic convergence.

For efficiency and robustness, the Jacobian is always discretized in a first-order manner, regardless of the order of accuracy of the residual. In this way, the diagonal dominance of the Lhs is ensured for any time step. An approximate inversion can then be carried out using a relaxation scheme. The equation for the subiterations reads

$$[L_i^-]\Delta Q_{i-1}^p + [L_i]\Delta Q_i^p + [L_i^+]\Delta Q_{i+1}^p = -R(Q^p, Q^n, Q^{n-1}), \tag{16}$$

where the $[L]$s represent the entry of a line:

$$[L_i^-]\Delta Q_{i-1} = -[A_{i-1/2,j}^+]\Delta Q_{i-1,j},$$

$$[L_i]\,\Delta Q_i = -[C_{i,j-1/2}^+]\Delta Q_{i,j-1} + [D_{i,j}]\Delta Q_{i,j} + [C_{i,j+1/2}^-]\Delta Q_{i,j+1},$$

$$[L_i^+]\,\Delta Q_{i+1} = [A_{i+1/2,j}^-]\Delta Q_{i+1,j},$$

$$[D_{i,j}] = \left[c_{n+1}\frac{h^{n+1}}{\Delta\tau} + A_{i+1/2,j}^+ - A_{i-1/2,j}^- + C_{i,j+1/2}^+ - C_{i,j-1/2}^- \right],$$

and where $c_{n+1} = \frac{3}{2}$ for a second-order scheme and $c_{n+1} = \frac{11}{6}$ for a third-order scheme. The exact Jacobian of the inviscid flux using Roe's FDS is very complicated and expensive to calculate, [see Barth (1987)], so that a simplified Jacobian is used instead, as follows:

$$A^{\pm} = \tfrac{1}{2}A(Q^{\pm}) \pm \tfrac{1}{2}|A(\bar{Q})| \quad \text{and} \quad C^{\pm} = \tfrac{1}{2}C(Q^{\pm}) \pm \tfrac{1}{2}|C(\bar{Q})|.$$

It may be expected that due to these approximations the convergence will be slower, but during numerical experiments the method performed well and turned out to be very robust.

When a local time step is applied on the Lhs, the time-stepping method becomes similar to the approach of Jameson (1991) in which an explicit subiteration scheme is employed. In this case the local time step should be set to

$$\Delta\tau = \min(\Delta\tau_{\text{global}}, \Delta\tau_{\text{ref}}/\lambda), \quad \lambda = |U| + |W| + a(|\nabla\xi| + |\nabla\zeta|).$$

Here temporal integration with a local time step is only needed to start the simulation. After a number of steps, a very large global time step may be used to obtain fast convergence to steady state.

In solving equation (16), a line relaxation is employed with direct inversion along ζ lines. The direct inversion should resolve stiffness due to the mesh stretching and implicitly handles the viscous terms which have an elliptic behavior. To account for the nature of signal propagation and for stability reasons when the Rhs is of higher-order accurate, forward and backward sweeps are carried out in ξ direction. The forward sweep from ξ_1 to $\xi_{\max}$ is

$$[L_i]\Delta\bar{Q}_i^{p+1} = -R_i - [L_i^-]\Delta\bar{Q}_{i-1}^{p+1} - \omega_l[L_i^+]\Delta Q_{i+1}^p,$$

which results in an intermediate solution $\Delta\bar{Q}$, followed by the backward sweep,

$$[L_i]\Delta Q_i^{p+1} = -R_i - \omega_l[L_i^-]\Delta\bar{Q}_{i-1}^{p+1} - [L_i^+]\Delta Q_{i+1}^{p+1},$$

where $\omega_l = 0{\cdot}80 - 0{\cdot}90$. Due to the differences of the Lhs with the exact Jacobian of the Rhs only a part of the correction is used to update Q: $Q^{p+1} = Q^p + \omega\Delta Q$, where $\omega = 0{\cdot}30 - 0{\cdot}60$.

When the iteration is started from a poor initial guess (e.g. the freestream condition) more than one iteration is needed before the residual is updated. After a number of time steps, the

residual is updated after every sweep to obtain faster convergence. In this case the scheme represents a nonlinear relaxation method and ω_l should be set to $\omega_n = 0{\cdot}30 - 0{\cdot}40$. The subiteration is stopped once $|R^{n+1,p}|$ drops below a prescribed value. This criterion is different from the one applied by Jameson (1991) where $|R^{n+1,p}|/|R^{n+1,0}|$ is used. The present choice has been made after having observed that sometimes in the beginning of a subiteration the value of the unsteady residual is already very small, so that setting the convergence criterion relative to this level would lead to an unnecessarily too stringent condition.

2.4. Grid Generation

The initial grids for the calculations carried out in this paper have been generated using a transfinite interpolation employing Hermite polynomials and an elliptic smoother similar to Thompson (1987). In the case of moving boundaries, the grid has to conform to the surface at each time step. For the results presented in this paper, rigid mesh motion has been employed because the chordwise flexibility is not considered. Flexible mesh motion employing the spring analogy of Batina (1989) has also been applied without any significant difference in the resulting pressure distribution.

3. AEROELASTIC EQUATIONS

The equations of motion of a rigid airfoil having two degrees of freedom, heaving and pitching about the elastic axis (h, α) , may be derived by balancing the force and moment about the elastic axis. This results in two equations:

$$\ddot{h} + x_\alpha \ddot{\alpha} + \omega_h^2 h = -2q_\infty C_L/m,$$
$$x_\alpha \ddot{h} + r_\alpha^2 \ddot{\alpha} + r_\alpha^2 \omega_\alpha^2 \alpha = 4q_\infty C_M/m,$$

where nondimensional structural parameters have been used. Since both aerodynamic and structural equations will be integrated simultaneously, the nondimensional time steps of these two sets of equations have to match. The characteristic time for the aerodynamic part, c/a_∞, is used for the whole set of equations, to arrive at

$$M\ddot{x}(t) + Kx(t) = B'U(x, t), \tag{17}$$

with

$$M = \begin{bmatrix} 1 & x_\alpha \\ x_\alpha & r_\alpha^2 \end{bmatrix}, \quad K = \frac{4M_\infty^2}{V^{*2}\mu} \begin{bmatrix} \omega_h^2/\omega_\alpha^2 & 0 \\ 0 & r_\alpha^2 \end{bmatrix},$$
$$B' = \frac{M_\infty^2}{\mu\pi} \begin{bmatrix} -4 & 0 \\ 0 & 8 \end{bmatrix}, \quad x = \begin{Bmatrix} h \\ \alpha \end{Bmatrix}, \mathrm{U} = \begin{Bmatrix} C_L \\ C_M \end{Bmatrix},$$

where V^* is the speed index. In case the accuracy of the structural part defines the time step for the whole set of aeroelastic equations, one might adopt the structural time, $\tau_s = t\omega_\alpha$. The scaling factor between aerodynamic and structural time steps is then $\Delta\tau_s = 2M_\infty/(V^*\sqrt{\mu}\Delta\tau)$. Equation (17) can be brought into a standard state-space representation as

$$\dot{X} = AX + BU, \tag{18}$$

where

$$A = \begin{bmatrix} 0 & I \\ -M^{-1}K & 0 \end{bmatrix}, \quad B = \begin{bmatrix} 0 \\ M^{-1}B' \end{bmatrix}, \quad X = \begin{Bmatrix} x \\ \dot{x} \end{Bmatrix}.$$

In the classical aeroelastic approach, the aerodynamic forces are divided into motion-dependent and motion-independent contributions (separation, wake, gust, etc.). Since in nonlinear cases this superposition principle cannot be applied, equation (17) treats the aerodynamic force as just one term, $U(X, t)$. Moreover, since in general the explicit relation between U and X can hardly be obtained in a simple manner, the aerodynamic forces will be treated as an excitation to the structural system; thus $U = U(t)$. The nonlinear coupling is effected via the boundary condition at the airfoil surface. The solution of equation (18) can be obtained using the standard matrix-transition method as

$$X^{n+1} = \Phi X^n + \Theta \bar{U}; \tag{19}$$

$\Theta \bar{U}$ represents the nonhomogeneous part of the solution of equation (18), where a constant aerodynamic force $\bar{U}$ is assumed between time level n and $(n + 1)$. See Edwards *et al.* (1982) for a detailed description of the method for aeroelastic applications. In the present study, a simpler method, namely the Newmark scheme with parameters resembling a trapezoidal scheme, is applied. This scheme is known to be neutrally stable, so that it does not introduce artificial damping. In this case, Φ and Θ are

$$\Phi = \left[I - \frac{\Delta\tau}{2} A \right]^{-1} \left[I + \frac{\Delta\tau}{2} A \right],$$
$$\Theta = \left[I - \frac{\Delta\tau}{2} A \right]^{-1} \Delta\tau B. \tag{20}$$

At the beginning of time step $(n + 1)$, $\bar{U}$ is approximated as $\bar{U} \approx \frac{3}{2} U^n - \frac{1}{2} U^{n-1}$. Subsequently, after an approximation of the position of the airfoil at $(n + 1)$ is obtained, U^{n+1} can be calculated to improve X^{n+1}, using $\bar{U} = \frac{1}{2}(U^n + U^{n+1})$.

4. RESULTS

The present method has been validated for unsteady flow applications, as well as steady flow ones.

4.1. Steady Flow

A steady viscous flow case of RAE2822 airfoil is considered at $M_\infty = 0{\cdot}729$, $\alpha_{\text{exp}} = 2{\cdot}92^\circ$, $\text{Re}_\infty = 6{\cdot}5 \times 10^6$ and a forced transition at 3% chord. Comparisons are provided by experimental data from Cook *et al.* (1979) and the Navier–Stokes method NLR-MUTU2D described in Haase *et al.* (1993). All calculations have been performed at a corrected angle of attack of $\alpha_{\text{corr}} = 2{\cdot}31^\circ$. Figure 1 shows the comparisons of distribution of pressure and friction coefficients. The comparison of the aerodynamic coefficients is shown in Table 1. Overall, good agreement is obtained between the results.

4.2. Unsteady Flow, Static Grid

The well-known unsteady flow test case of 18% circular arc airfoil of Seegmiller *et al.* (1978) is presented. The flow condition is $M_\infty = 0{\cdot}76$ and $\text{Re}_\infty = 11 \times 10^6$. The present result is obtained using a C-mesh of 140×60 with 100 points on the airfoil. The experiment was carried out in a curved-wall tunnel, while the calculation is performed with a freestream outer boundary at 10 chords away. The time history of the lift and moment coefficients is shown in Figure 2. This result was obtained using a time step of 0·10 with 8 subiterations per

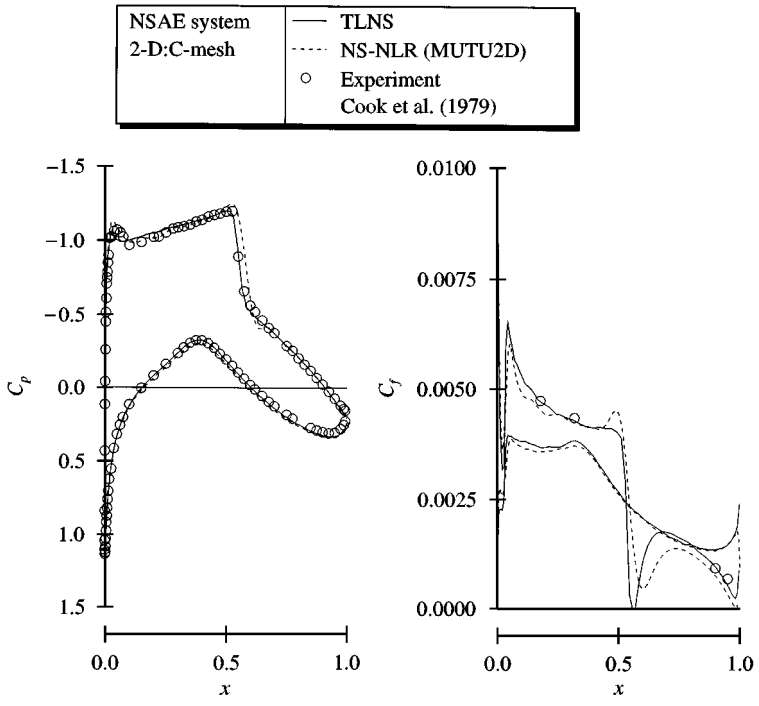

Figure 1. Comparison of calculated and experimental pressure coefficient and friction coefficient distributions for an RAE 2822 airfoil at $M_\infty = 0{\cdot}729$, $\alpha_{exp} = 2{\cdot}92°$ and $\alpha_{corr} = 2{\cdot}31°$; x is non dimensionalized with respect to c.

TABLE 1
Comparison of the aerodynamic coefficients of the present method, the NLR MUTU2D and the experiment of Cook *et al.* (1979)

	C_L	C_M	C_D
Present result	0·748	− 0·098	0·0150
NS-NLR (MUTU2D)	0·777	− 0·105	0·0149
Experiment	0·743	− 0·095	0·0127

time step producing a maximum CFL number of about 18 000; 500 time steps were needed to reach a nondimensional observation time of 50. The instantaneous Mach contour at four time levels are presented in Figure 3 showing the moving shocks, strengthening in upstream and weakening in downstream direction. The reduced frequency, which is calculated by identifying the period of oscillation, is presented in Table 2. The occurrence of unsteady flow like in the experiment and the agreement of the frequency give confidence in the time integration method and the modeling of turbulence.

4.3. Unsteady Flow, Forced Vibration

The responses of a rigid NACA0012 airfoil under forced vibrations are analysed here to asses the performance of the solver. The inviscid flow results were obtained using a grid with

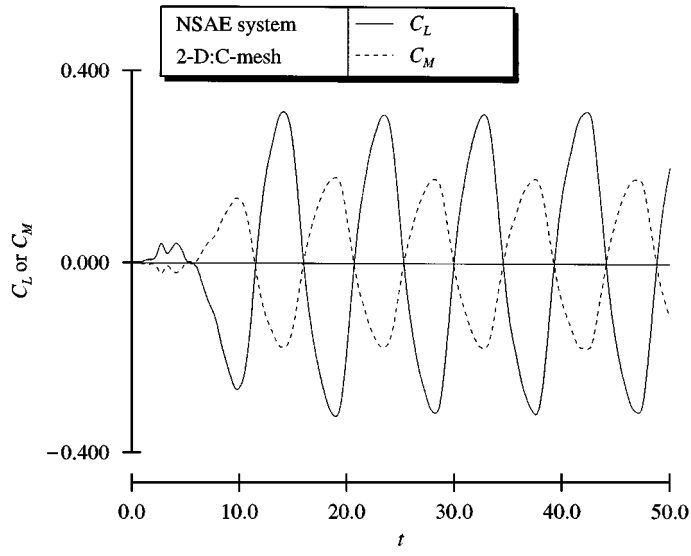

Figure 2. Time histories of lift coefficient, C_L, and moment coefficient, C_M, about the quarter-chord of an 18% circular arc airfoil at $M_\infty = 0{\cdot}76$ and $\mathrm{Re}_\infty = 11 \times 10^6$; t is nondimensionalized with respect to c/a_∞.

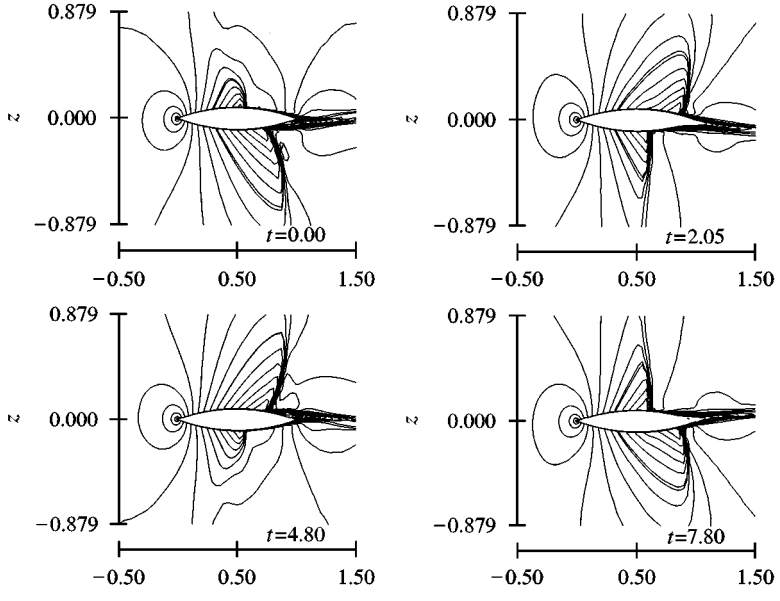

Figure 3. Instantaneous Mach contours at four time levels ($\Delta M = 0{\cdot}10$) of 18% circular arc airfoil at $M_\infty = 0{\cdot}76$ and $\mathrm{Re}_\infty = 11 \times 10^6$.

a size of 140×30 and the viscous flow calculations were carried out on a grid of 140×60. Both grids have 100 points on the airfoil surface. The outer boundary is placed at 40 chords from the airfoil. For the viscous flow calculations, the average distance of the first point away from the surface is about 6×10^{-6} chord.

TABLE 2
Comparison of reduced frequency obtained using the present method with the experiment of Seegmiller *et al.* (1978)

		k, based on chord
Present result	10 chords away freestream boundary	0·50
Experiment	Curved-wall tunnel	0·49

4.3.1. *NACA0012 airfoil, inviscid flow*

An example of an unsteady inviscid flow application of the method is shown in Figure 4. This is the case of an oscillatory pitching motion about the quarter-chord of the NACA0012 airfoil at transonic conditions, $M_\infty = 0{\cdot}754$, $\alpha_{\text{mean}} = 2{\cdot}00^\circ$, $\alpha_{\text{amp}} = 2{\cdot}50^\circ$ and $k = 0{\cdot}082$ based on semichord. This case reveals strong nonlinearities, since a strong shock is involved and the shock trajectory is significant. Results of the present method are compared with those of TULIPS, a full-potential flow method of Schippers (1988), an extended version of this method of Westland & Hounjet (1993) and an Euler method of DLR. The extended TULIPS method employs the Clebsch potential with entropy and vorticity corrections for the modeling of strong shock waves. The DLR-Euler method uses an explicit method to march in time; the description of the method can be found in Polz (1991).

Figure 4 shows the comparison of lift and moment coefficients. The results of the present method, the DLR-Euler method and the extended TULIPS method agree very nicely. The TULIPS full-potential flow result shows a consistent difference to the Euler results. The hardly noticeable difference between the results of the present implicit method and the explicit method of DLR confirms the applicability of the present time-stepping strategy. The present result was obtained using 48 time steps per period of oscillation, and at each time step 8 subiterations were employed. The time needed to run one period of oscillation was less than 2 min on a SGI (R8000/R8010 chips) workstation. The adequacy of the present method for the current case is presented in Figure 5 and in Table 3 which demonstrate the computational efficiency for several variations of the iteration strategy. The lift and moment coefficients show a very good agreement even for an extremely low number of steps per period.

4.3.2. *NACA0012 airfoil, viscous flow*

Two cases are considered in this section. The first case is again the NACA0012 airfoil at transonic conditions, $M_\infty = 0{\cdot}754$, $\text{Re}_\infty = 5{\cdot}7 \times 10^6$, $\alpha_{\text{mean}} = 2{\cdot}00^\circ$, $\alpha_{\text{amp}} = 2{\cdot}50^\circ$ and $k = 0{\cdot}082$. The experimental result is taken from Wood (1979). The transition was forced at 10% chord. Figure 6 shows the comparison of the experimental and the calculated results. It can be concluded that only during the up-stroke the lift and moment are reproduced relatively well. The discrepancy between the results starts near the maximum angle of attack and is most probably due to the inadequacy of the algebraic turbulence modeling to treat a strong shock properly. During the down stroke, only the second half is satisfactorily predicted.

Another application of the present TLNS solver is shown in Figure 7 for the AGARD standard test case of transonic viscous flow, case 3 of Landon (1982). The flow conditions are $M_\infty = 0{\cdot}60$, $\text{Re}_\infty = 4{\cdot}8 \times 10^6$, $\alpha_{\text{mean}} = 4{\cdot}86^\circ$ and the boundary layer is fully turbulent.

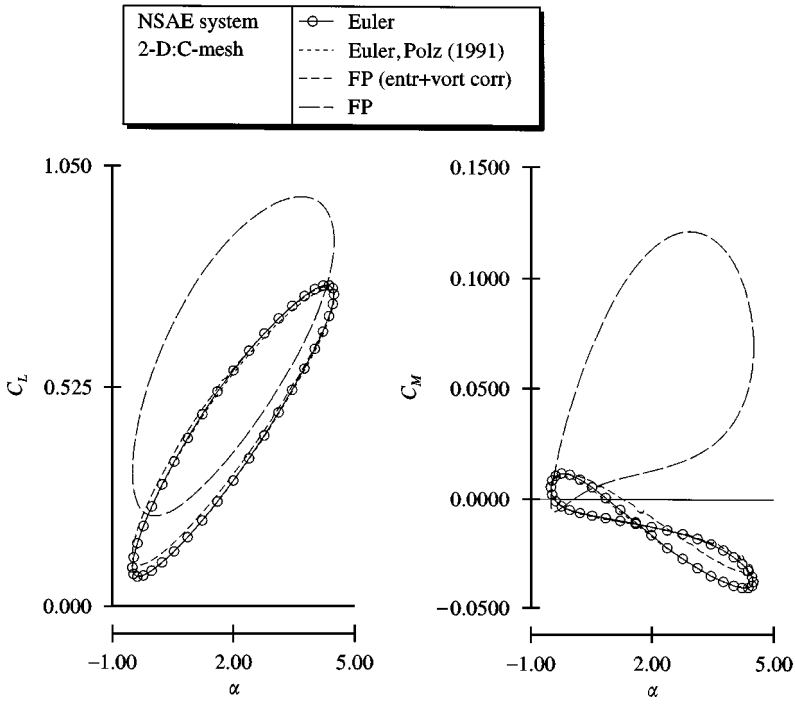

Figure 4. Comparison of calculated lift coefficient and moment coefficient about the quarter-chord of NACA0012 at $M_\infty = 0{\cdot}754$, $\alpha_{mean} = 2{\cdot}00^\circ$, $\alpha_{amp} = 2{\cdot}50^\circ$ and $k = 0{\cdot}082$, based on semichord.

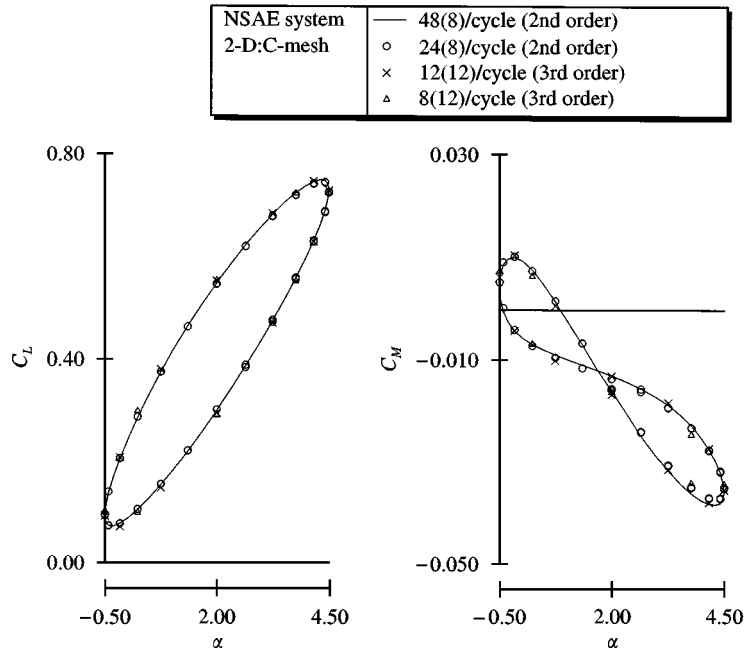

Figure 5. Comparison of lift coefficient and moment coefficient about the quarter-chord for a variety of iteration strategies of the inviscid flow case.

TABLE 3
CPU time comparison of running strategies for the inviscid flow case shown in Figure 5

$\Delta\tau$/period	Subiteration	$\partial Q/\partial\tau$	CPU-time (min/period)
48	8	2nd order	1·74
24	8	2nd order	0·87
12	12	3rd order	0·64
8	12	3rd order	0·43

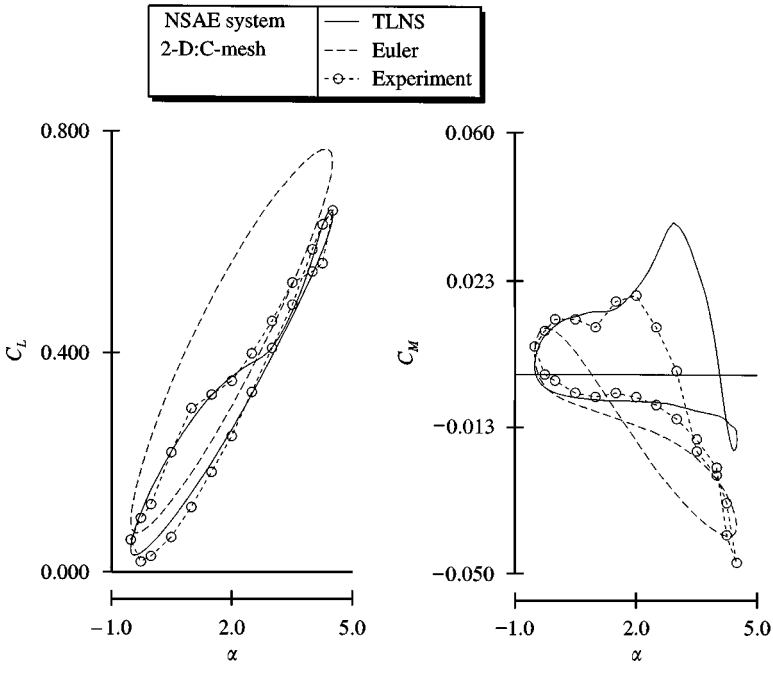

Figure 6. Comparison of calculated and experimental lift coefficient and moment coefficient about the quarter-chord during oscillatory pitching motion of a NACA0012. $M_\infty = 0{\cdot}754$, $\mathrm{Re}_\infty = 5{\cdot}7 \times 10^6$, $\alpha_{\mathrm{mean}} = 2{\cdot}00^\circ$, $\alpha_{\mathrm{amp}} = 2{\cdot}50^\circ$ and $k = 0{\cdot}082$, based on semichord.

The mode of vibration is a pitching oscillation about quarter-chord with an amplitude of $\alpha_{\mathrm{amp}} = 2{\cdot}44^\circ$ and $k = 0{\cdot}081$ based on semichord. Figure 7 shows the results of the test case. Excellent agreement of both calculated results is obtained for the lift and the moment coefficients. The agreement with the experimental data is also good, as far as the lift coefficient is concerned, but less satisfactory for the moment coefficient. The present results were obtained using 400 steps per period of oscillation with 4 subiterations in each time step. The CPU time was 35 min on a SGI (R8000/R8010 chips) workstation. The maximum CFL number during the calculation was about 55 000. The adequacy of the present method for the current case is presented in Figure 8 and in Table 4 where the computational efficiency is demonstrated for several iteration strategies. The lift coefficient shows a very good agreement even for a very low number of steps per period. The moment coefficient shows a more sensitive behaviour. Some differences are apparent, but the extremities appear to be captured well enough by all strategies. It is generally known that the result obtained

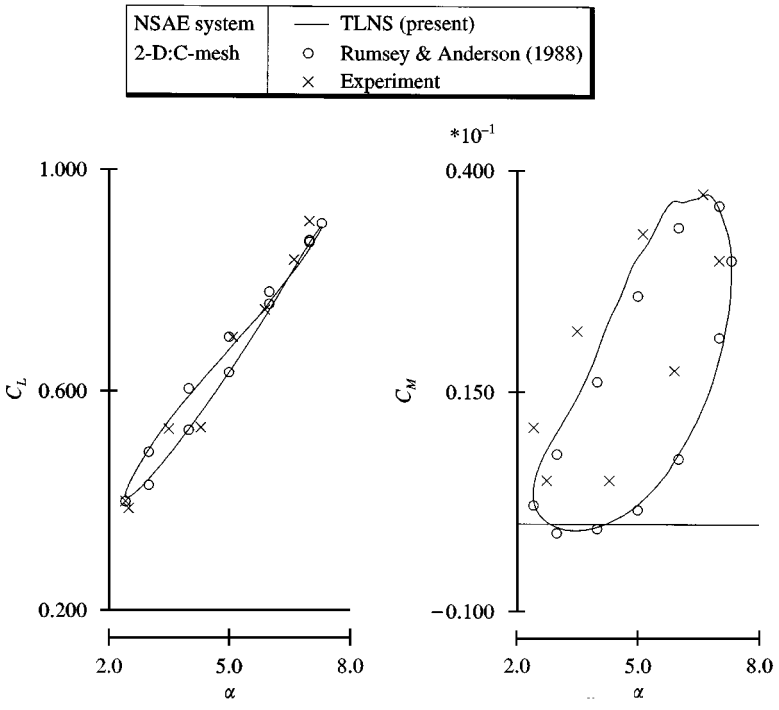

Figure 7. Comparison of calculated and experimental lift coefficient and moment coefficient about the quarter-chord during oscillatory pitching motion of NACA0012 at $M_\infty = 0{\cdot}60$, $\mathrm{Re}_\infty = 4{\cdot}8 \times 10^6$, $\alpha_{\mathrm{mean}} = 4{\cdot}86°$, $\alpha_{\mathrm{amp}} = 2{\cdot}44°$ and $k = 0{\cdot}081$, based on semichord.

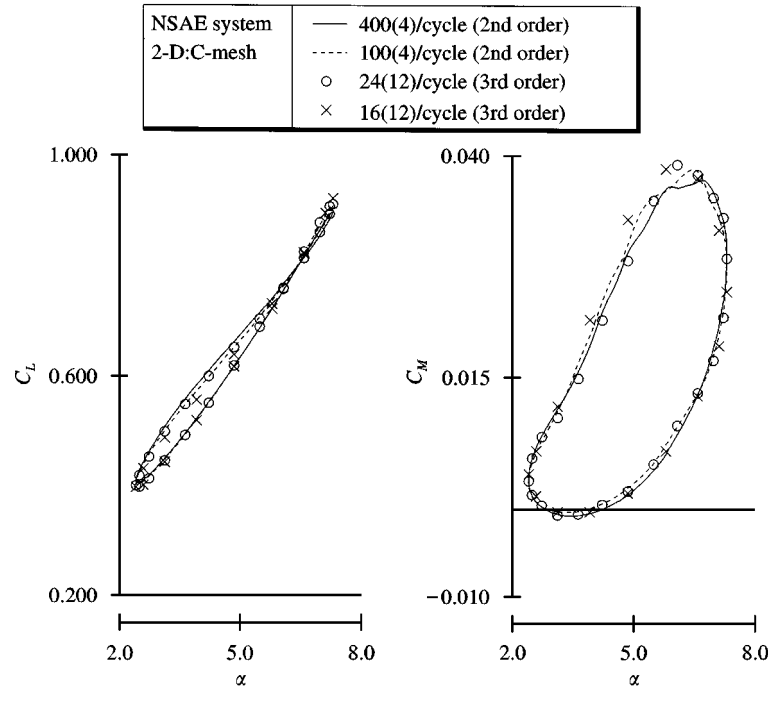

Figure 8. Comparison of lift coefficient and moment coefficient about the quarter-chord for a variety of iteration strategies for the viscous flow case.

TABLE 4
CPU time comparison of running strategies for the viscous flow case shown in Figure 8

$\Delta\tau$/period	subiteration	$\partial Q/\partial\tau$	CPU-time (min/period)
400	4	2nd order	35·45
100	4	2nd order	8·83
24	12	3rd order	6·25
16	12	3rd order	4·46

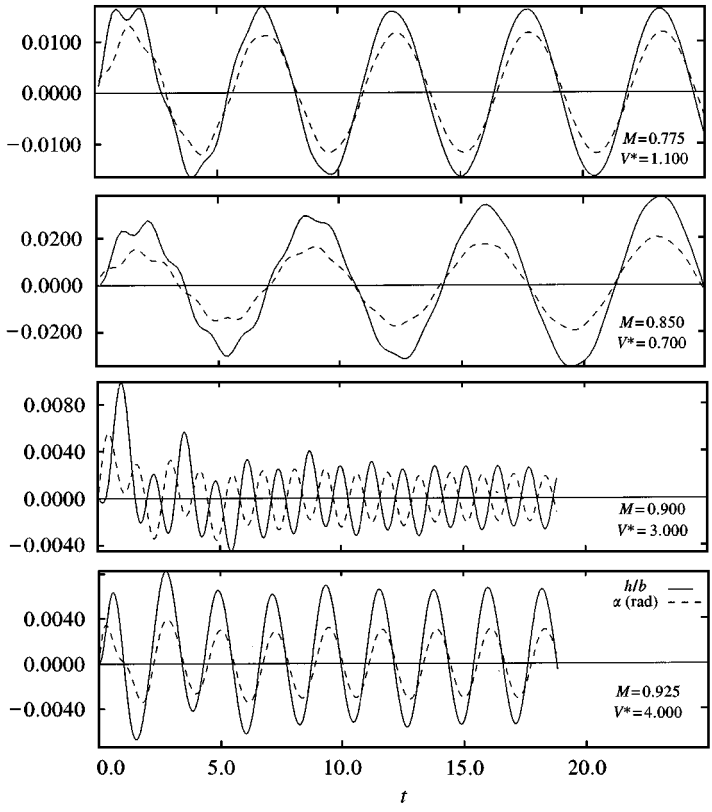

Figure 9. Time responses close to the flutter boundary for the inviscid flow case.

with FDS needs less grid points. compared to flux-vector splitting (FVS) which is more diffusive and therefore more robust. The results of Rumsey & Anderson (1988) were obtained using FVS to obtain large time step. The present result was obtained using FDS (with a coarser grid) and moreover with a larger time step, thus a saving compared to the method of Rumsey & Anderson (1988) is obtained.

4.4. AEROELASTIC CASE

In this section, a flutter analysis is applied to a NACA64A010 airfoil moving in two degrees of freedom. The test case A of Isogai (1981) is considered with the following nondimensional

structural parameters, $a = -2{\cdot}00$, $x_\alpha = 1{\cdot}80$, $r_\alpha^2 = 3{\cdot}48$, and a ratio of uncoupled frequencies $\omega_h/\omega_\alpha = 1{\cdot}00$. The value of a shows that the elastic axis is located half a chord in front of the leading edge which represents a typical section for a swept wing. The wind-off coupled frequencies are $0{\cdot}7134\omega_\alpha$ and $5{\cdot}338\omega_\alpha$. In case of viscous flow, the Reynolds number is $\mathrm{Re}_\infty = 6 \times 10^6$. The mass ratio is $\mu = 60$. The analysis proceeds by first calculating the steady-state condition at a certain Mach number. The airfoil is then excited sinusoidally in a pitching mode about the elastic axis at the frequency ω_α and with an amplitude of 1.00°. After 2 periods of forced oscillation, the airfoil is set free for another 4 to 5 periods to obtain the response.

The time needed for one run is about 15 min for an inviscid flow computation and about 90 min for a viscous flow computation. The viscous flow case takes much longer CPU time since it needs a smaller time step and also a finer grid.

The obvious consequence of an aeroelastic case is that the grid and metrics have to be recalculated not only at each time step but also during subiterations to arrive at a fully converged aeroelastic solution. From numerical experiments it turned out that the recalculation of grid and metrics at the subiterations is not needed for viscous flow calculations, because then the time step which is determined by the accuracy of the aerodynamic part is relatively small. When inviscid flow simulations are performed which involve relatively large time steps, only one correction is applied, and the method resembles a predictor–corrector scheme for the aeroelastic equations. Figures 9 and 10 show typical time responses close to the lowest flutter boundary at various Mach numbers

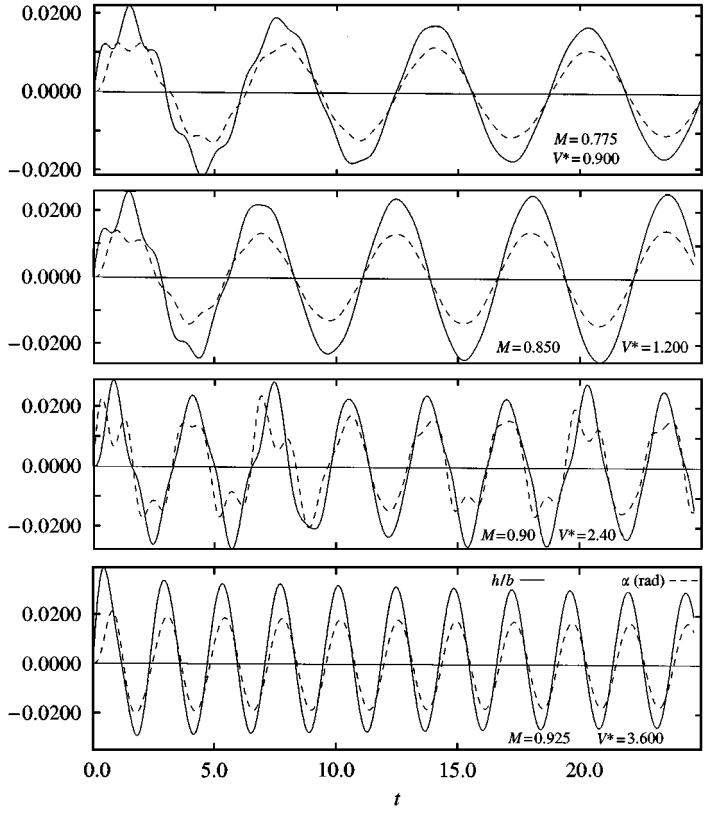

Figure 10. Time responses close to the flutter boundary for the viscous flow case.

for inviscid and viscous flows. The mode depicted by heave and pitch at almost the same phase is mostly bending with the node in front of the elastic axis. For both cases, by the increase of Mach number, the node moves towards the airfoil. An exception is for the inviscid flow response at $M_\infty = 0{\cdot}90$, where the mode is mostly rotation about a center at the airfoil.

Figure 11 compares the flutter speed indices obtained using the present inviscid flow method with inviscid flow results obtained by Isogai (1981) using a TSD method

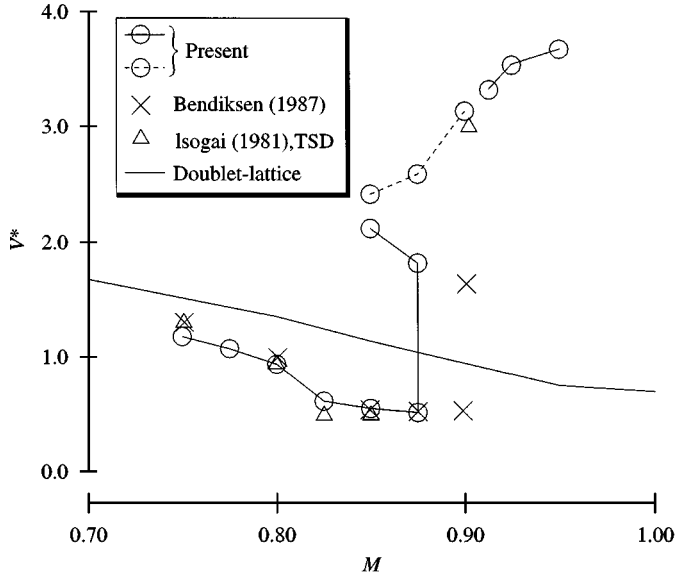

Figure 11. Comparison of calculated flutter boundaries for the inviscid flow.

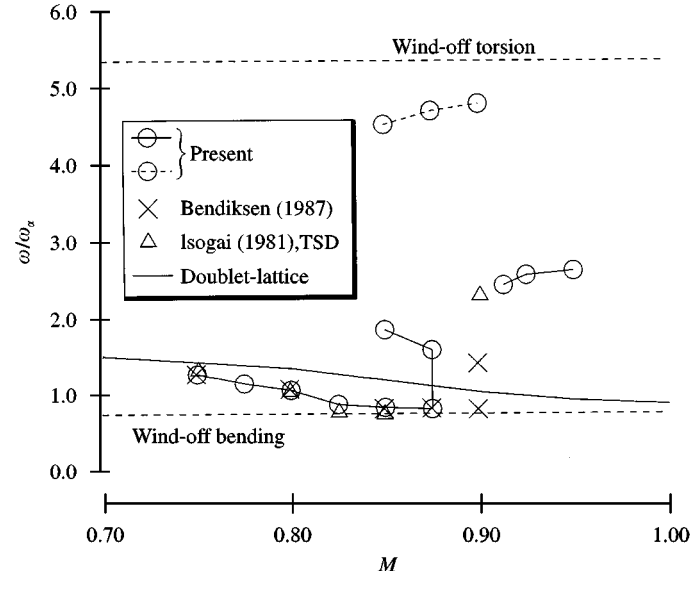

Figure 12. Comparison of calculated nondimensional frequencies at the flutter boundaries for the inviscid flow.

and by Bendiksen & Kousen (1987) using an Euler method. As a reference, calculations using linear thin-airfoil theory are also presented. Flutter speed indices were calculated starting from $M_\infty = 0{\cdot}75$ to $M_\infty = 0{\cdot}95$, with an increment of 0·025. The present inviscid flow results compare fairly well with the other results. The bottom of the dip is predicted at $V^* = 0{\cdot}53$, which is close to the TSD result. Until $M_\infty = 0{\cdot}875$ the lowest flutter is primarily due to the first mode which is mainly bending with a frequency close to the first coupled wind-off frequency. Thereafter a bulge occurs causing multiple flutter points. At $M_\infty = 0{\cdot}90$ the flutter is now primarily due to the second mode, which is mainly rotation. This situation can be seen from the time response of Figure 9.

Figure 11 shows that the second mode flutter starts already from $M_\infty = 0{\cdot}85$ at a speed index higher than the first mode flutter. It should be noted that the flutter point at $M_\infty = 0{\cdot}90$ and the adjacent one at $M_\infty = 0{\cdot}9125$ have a very different character, the first representing primarily the second mode and the latter primarily the first mode. This difference cannot be seen from Figure 11 but is indicated clearly in Figure 12. Figure 13 shows the comparison between the viscous and inviscid flow results. The viscosity apparently reduces the dip, fills up the bulge and passes the higher-frequency mode found in inviscid flow.

5. CONCLUSIONS

A method to solve the Thin-Layer Navier–Stokes/Euler equations for two-dimensional aeroelastic applications has been presented. The method employs large time steps, $\mathcal{O}(10)$ per period, while accuracy is maintained by solving the nonlinear unsteady equations using subiterations.

The results of the method demonstrate an adequate quality for a wide spectrum of two-dimensional applications.

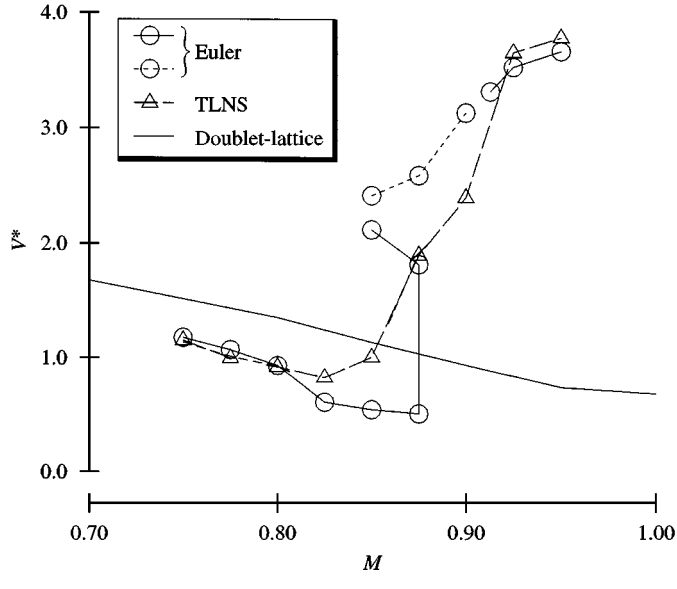

Figure 13. Comparison of calculated flutter boundaries of the viscous and inviscid flow cases.

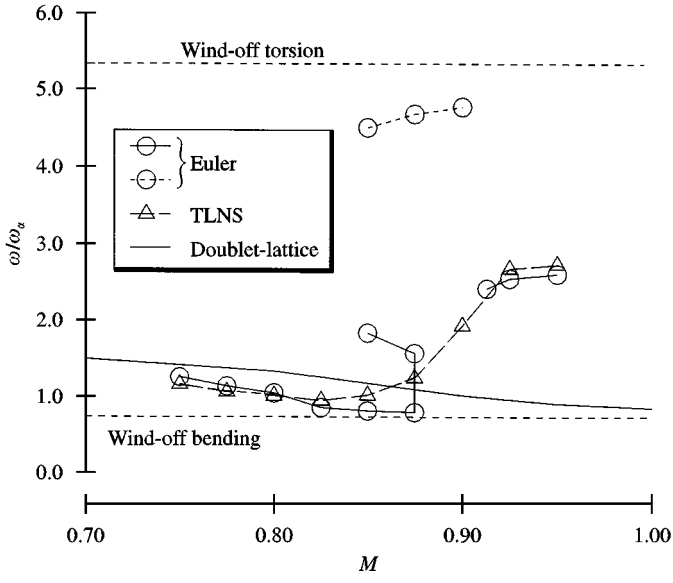

Figure 14. Comparison of calculated nondimensional frequency at the flutter boundaries of the viscous and inviscid flow cases.

The computational requirements admit two-dimensional aeroelastic simulations to be performed on a routine basis. The efficiency is obtained mainly from the freedom to take large time steps during the simulations.

The present method will be further developed and exploited for the study of flow characteristics of aeroelastic phenomena involving strong viscous interactions in transonic flow.

ACKNOWLEDGMENT

The authors would like to thank Prof. H. W. M. Hoeijmakers for encouragement and valuable discussions. Mr Prananta's stay in The Netherlands is sponsored by the Dutch–Indonesian cooperation program through the APERT project.

References

Alonso, J. & Jameson, A. 1994 A fully-implicit time-marching aeroelastic solution. AIAA Paper 94–0056

Alonso, J., Martinelli, L. & Jameson, A. 1995 Multigrid unsteady Navier–Stokes calculations with aeroelastic applications. AIAA Paper 95–0048.

Baldwin, B. & Lomax, H. 1978 This layer approximation and algebraic model for separated turbulent. AIAA Paper 78–0257.

Barth, T. 1987 Analysis of implicit local lineralization techniques for upwind and TVD algorithm, AIAA Paper 87–0595.

Batina, J. 1989 Unsteady Euler algorithm with unstructured dynamic mesh for complex-aircraft aeroelastic aalysis. AIAA Paper 89–1189.

Bendiksen, O. & Kousen, K. 1987 Transonic flutter analysis using the Euler equations. AIAA Paper 87–0911.

Haase, W., Brandsma, F., Elsholz, E., Leschziner, M. & Schwamborn, D. 1993 EUROVAL: an European iniative on validation of CFD codes. *Notes on Numerical Fluid Mechanics* **42,** pp. 89–99. Braunschweig: Vieweg Verlag.

Cook, P., Donald, M. M. & Firmin, M. 1979 Aerofoil RAE 2822 pressure distributions, boundary layer and wake measurem,ent. Experimental Data Base for Computer Program Assessment, AGARD AR-138. A6-1-A6-77.

Edwards, J., Bennett, R., Jr, W. W. & Seidel, D. 1982 Time marching transonic flutter solutions including angle of attack effects. AIAA Paper 82–0685.

Gear, C. 1971 *Numerical Initial Value Problem in Ordinary Differential Equations*, Series in Automatic Computation, Englewood Cliffs: NJ Prentice-Hall.

Guruswamy, G. 1990 Vortical flow computations on swept flexible wings using Narier–Stokes equations. *AIAA Journal* **28,** 2077–2084.

Guruswamy, G. 1991 Transonic aeroelastic computations on wings using Navier–Stokes equations. In Transonic Unsteady Aerodynamics and Aeroelasticity, AGARD CP-507, pp. 22.1-22.22.

Hounjet, M. & Eussen, B. 1994 Outline and application of the NLR aeroelastic simulation method. In *Proceedings of 19th Congress of ICAS*. pp. 1418–1441.

Ide, H. & Shankar, V. 1987 Unsteady full potential aeroelastic computations for flexible configurations. AIAA Paper 87–1238.

Isogai, K. 1981 Transonic dip mechanism of flutter of sweptback with. Part II. *AIAA Journal* **19,** 1240–1242.

Jameson, A. 1991 Time dependent calculations using multigrid, with applications to unsteady flows past airfoils and wings. AIAA Paper 91–1596.

Kouisen, K. & Bendiksen, O. 1988 Nonlinear aspects of the transonic aeroelastic stability problem. AIAA Paper 88–2306.

Landon, R. 1982 NACA 0012 oscillatory and transient pitching. Compendium of Unsteady Aerodynamic Measurement, AGARD R-702, 3-1-3-25.

Lee-Rausch, E. M. & Batina, J. T. 1993 Wing flutter bnoundary prediction using unsteady Euler method. AIAA Paper 93–1422.

Obayashi, S. 1992 Freestream capturing for moving coordinates in three dimensions. *AIAA Journal* **30,** 1125–1128.

Polz, G. 1991 Current European rotorcraft research activities on development of advanced CFD methods for the design of rotor blades (BRITE/EURAM 'DACRO' Project). In *Proceedings of 17th European Rotorcraft Forum*, pp. 39.1-39.10.

Prananta, B. B. & Hounjet, M. H. L. Aeroelastic simulation with advanced CFD methods in 2-D and 3-D transonic flow. In *Proceedings of 1996 Unsteady Aerodynamics Conference* pp. 7.1-7.14. London: RAeS.

Prananta, B. B. & Hounjet, M. H. L. Large time step aero-structural coupling procedures for aeroelastic simulation, In *Proceedings of 1997 CEAS International Forum on Aeroelasticity and Structural Dynamics*, pp. 63–71. Rome: AIDAA.

Rausch, R. D., Batina, J. T. & H. T. Y. Yang 1992 Three-dimensional time marching aeroelastic analyses using an unstructured-grid Euler method. AIAA Paper 92–2506.

Roe, P. 1981 Approximate Riemann solver, parameter vector, and difference schemes. *Journal of Computational Physics* **43,** 357–372.

Rumsey, C. & Anderson, W. 1988 Some numerical and physical aspects of unsteady Navier–Stokes computations over airfoils using dynamic meshes. AIAA Paper 88–0329.

Schippers, H. 1988 TULIPS: A method to calculate transonic potential flow about oscillating airfoils. NLR Report TR-88193.

Seegmiller, H., Marvin, J. & Levy, JR, L. 1978 Steady and unsteady transonic flow. *AIAA Journal* **16,** 1262–1270.

Swanson, R. & Turkel, E. 1993 Aspects of a high resolution scheme for Navier–Stokes equations. AIAA Paper 93–3372.

Thomas, P. & Lombard, C. 1979 Geometric conservation law and iats application to flow computations on moving grids. *AIAA Journal* **17,** 1030–1037.

Thompson, J. 1987 A general three-dimensional elliptic grid generation system on a composite block-structure. *Computer Methods in Applied Mechanics and Enginering* **64,** 377–411.

Westland, J. & Hounjet, M. 1993 Clebsch variable model for unsteady, inviscid, transonic flow with srong shock waves. AIAA Paper 93–3025.

Wood, M. 1979 Results of oscillatory pitch and ramp tests on the NACA0012 blade section. ARA Memo 220.

Wu, J., Kaza, K. & Sankar, L. 1989 Technique for the prediction of airfoil flutter characteristics in separated flow. *AIAA Journal* **26,** 168–177.

APPENDIX: NOMENCLATURE

a	speed of sound; offset EA downstream of semichord, normalized by b
b, c	semichord, chord
C_L	lift coefficient
C_M	moment coefficient, positive nose up
h	inverse Jacobian (J^{-1}); vertical displacement of EA, normalized by b
I_α	moment of inertia about EA, $= mb^2 r_\alpha^2$
k	reduced frequency, $\omega b/V_\infty$, kinetic energy, $= \frac{1}{2}(u^2 + w^2)$
K_h, K_α	stiffness constants
Pr	Prandtl number, $= \mu C_p/k$
Re,Re	Reynolds numbers, $= \rho V_\infty c/\mu$, $\rho a_\infty c/\mu$
r_α	radius of gyration, nondimensionalized by b
V^*	speed index, $= V_\infty/(b\omega_\alpha\sqrt{\mu})$
x	$[h, \alpha]^T$
x_α	offset EA downstream of CG, normalized by b
γ	specific heat ratio, $= 1{\cdot}4$
μ	mass ratio, $m/(\pi\rho b^2)$, coefficient of viscosity, $\mu = \mu_L + \mu_T$
ω_h, ω_α	uncoupled frequencies